

Polarimetric Hyperspectral imaging Systems and Applications

Li-Jen Cheng, Colin Mahoney, George Reyes, and Clayton LaBaw
Center for Space Microelectronics Technology
JPL Propulsion Laboratory
California Institute of Technology
Pasadena, CA 91109

and

G.P. Li
Department of Electrical and Computer Engineering
University of California
Irvine, CA 92717

This paper reports activities in the development of AOTF Polarimetric Hyperspectral imaging (PII) systems at JPL along with field observation results for illustrating the technology capabilities and advantages in remote sensing. In addition, the technology was also used to measure thickness distribution and structural imperfections of silicon-on-silicon wafers using white light interference phenomenon for demonstrating the potential in scientific and industrial applications.

1. Introduction

The noncollinear acousto-optic tunable filter (AOTF) was invented by I. C. Chang¹. Functionally, the AOTF is a real-time programmable high-resolution spectral bandpass filter with polarization beamsplitting capability. **with** proper optics and focal plane arrays, one can build a polarimetric hyperspectral imaging (PII) system capable of measuring spatial, spectral, and polarization characteristics of a target with a single instrument.

We developed an AOTF-PII prototype system operating in a wavelength range of 0.48-0.75 microns² and did a number of outdoor field experiments which demonstrated unique advantages of using AOTF-PII in remote sensing applications. In addition, we investigated the potential applications of the AOTF technology in the non-remote sensing areas, specifically, in the area of semiconductor materials characterization.

Currently, we are in the process to develop an AOTF-P111 prototype system operating in the short-wave infrared range of 1.2-2.4 micron with the objective to demonstrate the technology capability from an airborne platform for USA SS1 DC.

2 Ground Prototype System

The P111 system contains an optical subsystem, two integrating CCD cameras, a RF generator and a power amplifier, a PC computer for control and data acquisition, and monitors. The unique part of the system is the optical configuration as illustrated in Figure 1.

The system contains a 3 inch aperture, zoom telelens set with variable focal length of 80-200 mm as the objective lens; an aperture located at the objective lens image plane for allowing only photons from the desired scene to pass through; a collimating lens to create an intermediate pupil plane whose cross section is comparable with that of the AOTF locating at the pupil plane; a field lens to create adequate beam diversion for imaging at the cameras; and two cameras for recording two polarized images simultaneously.

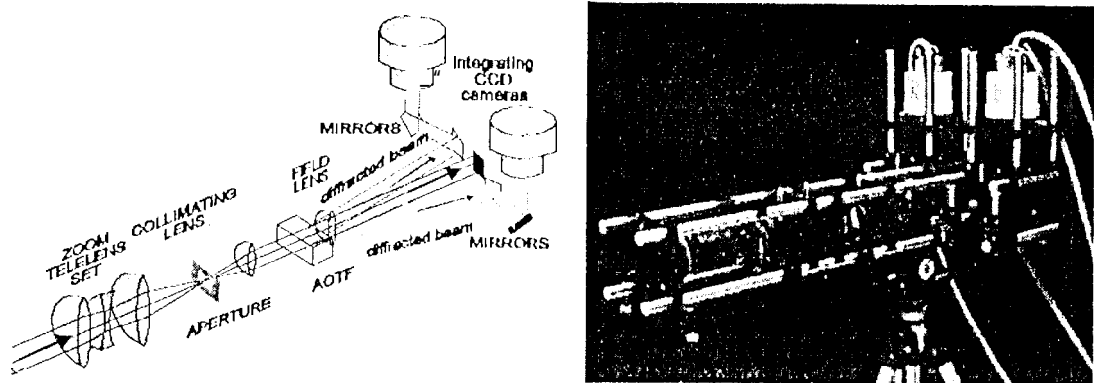


Figure 1. Left: Schematic diagram of the system optical configuration
Right: Photo of the optical system without the cover.

3 Remote Sensing Results

3.1 Field Observations at Ft. Huachuca, AZ

Figure 2 gives a grayscale image of the scene taken by an ordinary 35 mm camera. The scene contained a variety of typical southern Arizona plants and a small number of Army facilities. The observation condition and data processing techniques were given in a previous paper³. In this report, the important observations are given. There was a reflection reference plate of BaSO₄ observable as a small bright rectangular object in the upper left part of the picture,

that was used for intensity normalization. The distance between the plate and the instrument was about 3.6 km. The observation was carried at the noon time of a sunny day. The atmosphere was clear with observable haze only when one looked at distant objects. The instrument directed at the north with 12 degrees off to the east.

3. J. 1 Results

3.1.1.1 Vegetation Signatures

Figure 3 gives a spectral image of the scene at 0.67 μm at which the chlorophyll absorption is at maximum. Consequently, oak trees appeared to be dark, whereas mesquites were in gray. In general, all dark and gray areas were related to vegetation. The bright areas contained mainly dry grass and bare soil. Figure 4 gives reflected intensity spectra of oak and mesquite located in the lower left part of the scene, illustrating that the reflectance of oak is considerably lower than that of mesquite in the 0.62-0.69 μm wavelength range, consistent with the observed image.



Figure 3. Spectral image at 0.67 μm .

The observed spectra also show a sharp rise in the reflectance between 0.69 and 0.73 μm , due to chlorophyll, illustrating an effective way to map vegetation using

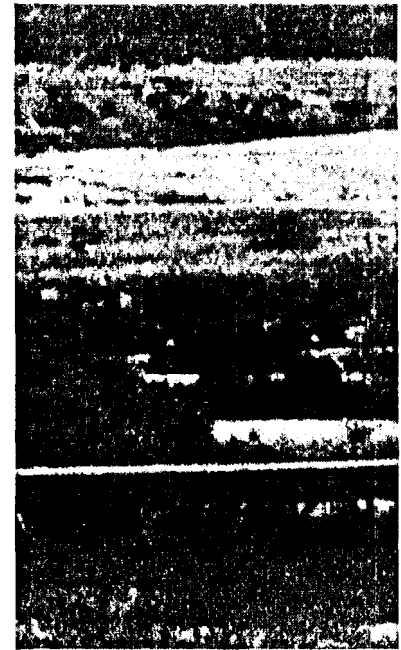


Figure 2. Grayscale image of the scene

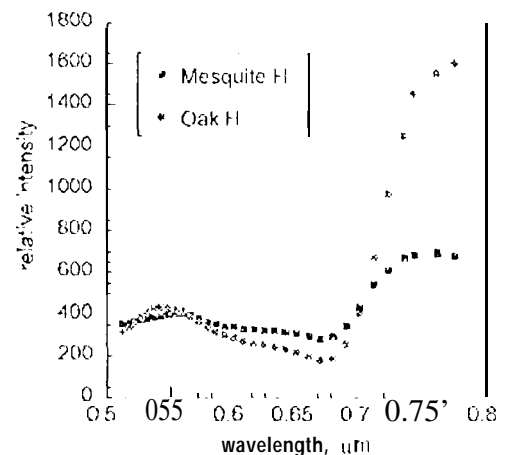


Figure 4. Reflectance spectra of oak and mesquite with horizontal polarization.

spectral derivatives. Figure 5 gives a spectral derivative image of the scene at 0.71 μm . Bare ground and dry grass are often bright objects in the intensity image. Because of lack of chlorophyll, they become dark in this wavelength range. The brightness in the spectral derivative image mainly relates to leaf chlorophyll concentration. Therefore, the spectral derivative image is an effective approach for monitoring health state and stress response in vegetation.

2.1.1.2 Polarization Signatures

Polarization is an important parameter for analyzing signatures of objects obtained from a remote sensing instrument. The AOTF system provides two spectral image set with linear polarization directions orthogonal to each other. The data reported here were taken with polarization parallel and perpendicular to the ground. So we defined the measured polarization to be $(I_v - I_h)/(I_v + I_h)$ where I_v and I_h are intensities at a same pixel of vertical and horizontal polarization images, respectively.

Figure 6 gives measured polarization spectra of oak, mesquite, and a unknown tree for illustrating some interesting, spectral polarization features of tree leaves.

It is well known that vegetation has polarization signatures. The data in Figure 7 have revealed that leaves of these trees have a similar polarization spectral signature, namely a sharp descending step at 0.69 μm beyond which the signal is low. This descending step coincides with the increase of the red absorption edge. The observation suggests that the sharp decreasing feature could be related to the chlorophyll.

Figure 7 gives the polarization image at 0.56 μm . The polarization image quality was more sharper than that of spectral images. The loss of the spatial resolution in the spectral images can be attributed to be spectral mixing due to light scattering among neighboring objects.⁴

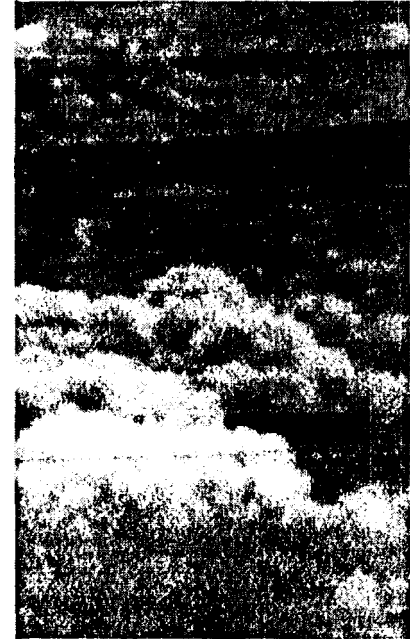


Figure 5. Spectral derivative image of the scene at 0.71 μm with horizontal polarization.

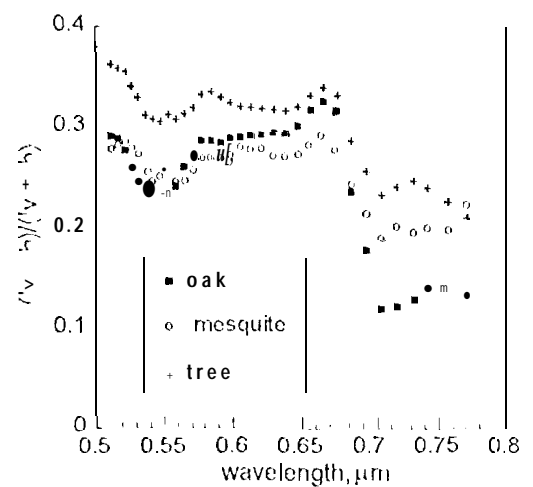


Figure 6. Polarization spectra of oak, mesquite, and unknown tree.

2.1. 1. Target Detection

This polarization image has an inverse triangular dark pattern at the location left from the center of the scene. The pattern was composed several different objects. Each object has its own spectral dependence. Around 0.56 μm , they appealed together as the observed pattern.

In the color picture taken by a 35 mm camera, the top corresponding part of the observed pattern is a small diamond-shape open area surrounded by the brushes. However, in the enlarged polarization image of Figure 8, only the brushes at the left had normal vegetation polarization signal. There were two short dark line segments along the 'brush' edges at the upper, right, and lower sides of the open area. The darkness of the line segments indicated strongly that their origin must be some materials different from those of the vegetation. The neighboring area at the upper, right, and lower parts of the segments was also darker in comparison with the brush signal. These observations suggest that the line segments and some of their surrounding were man-made objects.

In the color image, the rest of the target appeared to be bright green trees with two separated green spherical objects. In the polarization picture, the spherical objects were very dark dots with a dark line between them forming a dumbbell pattern. The dumbbell pattern is likely to be a man-made object. In addition, in the polarization picture, the image of the 'green tree' area was composed with several broad horizontal gray line segments arranged in the shape of an inverted acute triangle.

These contradicting observations between the color and spectral polarization images, we concluded that we detected a camouflaged target area. A detailed observation at the enlarged picture provided a verification that the 'green tree' was green camouflage nets covering unknown objects and neighboring tree tops. The detection was mainly due to the spectral polarization imaging capability of the AOTF-PHI system. It ought to note that the lower part of the pattern was also



Figure 7. Spectral polarization image at 0.56 μm .

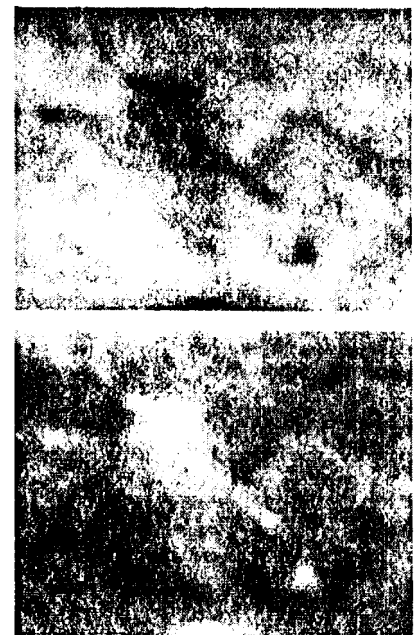


Figure 8. Enlarged positive (upper) and negative (lower) images of the pattern.

observable in spectral images of green wavelengths. However, the spectral polarization data provided the evidence for the determination of the target being camouflaged.

3.1.1.4 *Aerosol Scattering Effects*

The existence of atmospheric boundary-layer aerosols affects the magnitude, shape, and polarization of the spectra. The effects become substantial in the observation of distant objects. The measured differences in intensity, spectrum, and polarization due to the distance can provide important information about the aerosol. Using spectral and polarization data of two oak trees located at different distances from the instrument, we obtained the wavelength dependence of the scattering in the air at the observation site, from which one can obtain a smooth inverted wavelength power function, normally used to characterize light scattering in the atmosphere. More information on this subject was given previously.³

3.2 **Mine Detection in An Iceplant Field**⁴

Figure 9 gives a grayscale image of an iceplant field scene with a group of targets of interest whose locations were indicated in a sketch at the right. The targets included seven inactive mines: one green square plastic (D), two green round metallic (A and C), two dark green round metallic (G and H), and dark brown round metallic (I and J). Some mines were placed on the top of the implant and some were pushed into the iceplant field so that only a portion of the target was visible. In addition, there were two partially observable cement blocks (B and F), and one buried white plastic pipe with one foot length being observable (E). The iceplant field was a mixture of healthy and dead iceplants with uneven distribution. In addition, portions of healthy iceplants were in blossom with orange flowers. This arrangement did provide an interesting challenge for testing the system capability.

The right upper corner of the scene were a pile of metallic sheets and parts whose images were removed during the data analysis so that we can obtain a better dynamic range in the area of interest. Two Halon plates (K and L) of the Lambertian surface reflectance over the instrument wavelength range were also placed in the scene for intensity normalization among different wavelengths. The 111 system was on the top of a small hill and looked at the area with a downward angle of about 30 degrees and directed at 210 degrees south. The observation was carried out at the noon. The iceplant field was located about 40 meter away from the system and on a small plateau of the hill. The weather was sunny with typical Los Angeles basin smog in June.

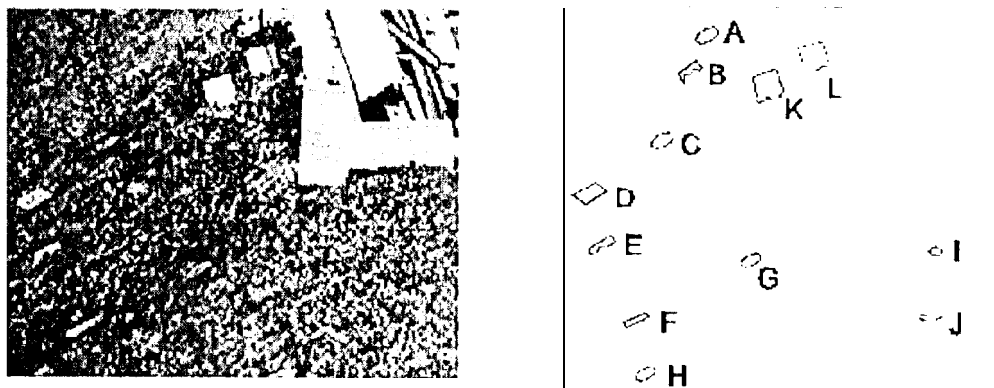


Figure 9. Left: Image of the iceplant field taken with an ordinary camera. Right: Sketch of locations of objects of interest in the iceplant field,

After image processing, we found that all the mines in the polarization difference images at the green wavelength range appeared as bright spots, whereas other objects were more difficult to be seen, as illustrate in Figure 10.

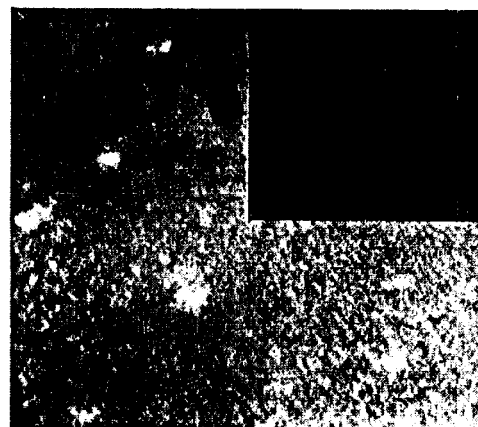


Figure 10. Polarization difference image at 0.55 micron illustrating that mines appear to be bright spots,

4* Non-remote Sensing Applications

4.1 Characterization of Silicon-On-Insulator (SOI) Wafers⁶

We successfully demonstrated the use of 111 I 10 measure white light interference at the sample as a non-invasive characterization tool for SOI wafers. The samples were silicon-on-silicon wafers manufactured by subsidiaries of Hughes and IBM. The results have illustrated the 111 capability of providing high-resolution thickness maps of both Si and oxide layers with high accuracy and observing optically active imperfections and distributions in the SOI structure.

Each point on the wafer has its own interference spectrum plus a DC background. The DC component was removed for obtaining the interference amplitude spectrum (Figure 11). By comparison of the spectrum with the result from an

interference model, the layer thickness of silicon and oxide each location was obtained. In addition, a correlation function between the measured spectrum and that predicted from the model was also computed. This process provides a correlation map from which the structure imperfections can be detected and located. Figure 12 gives measured thickness maps for silicon and oxide layers at one sampled area as well as the correlation factor between the experimental spectrum and that predicted by the model. The means and standard deviations of silicon and oxide thickness and the correlation factor are shown at the lower part of the figure. The black spot in the correlation image was a serious structure imperfection.

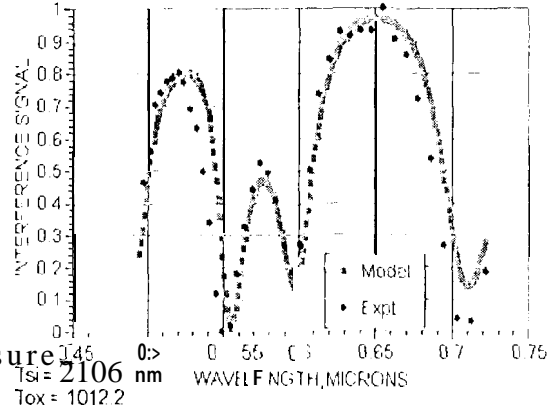


Figure 11. Comparison of theoretical and experimental interference spectra for obtaining the thickness of Si and oxide layers.

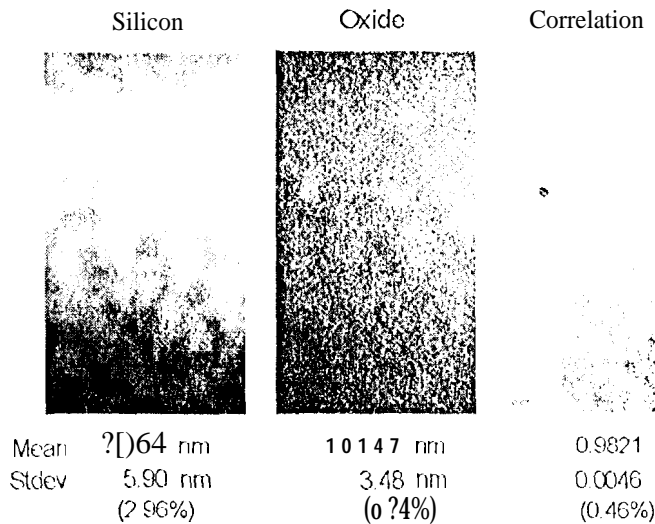


Figure 12. Silicon and oxide thickness distributions obtained from white light interference images as well as the correlation factor distribution of model prediction and measured data. The black spot in the correlation image reveals a serious structure imperfection at the location.

4.2 Microscopic

An optical connection between the PII system and a microscope was successfully made. This allowed us to obtain PII images of small objects commonly observed only under a microscope. Figure 15 gives a pair of images on a field-effect transistor in an integrated circuit chip at two orthogonal polarization conditions.

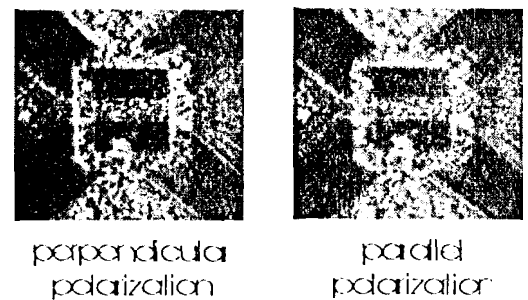


Figure 13. PII images of a FET device in an integrated circuit chip at 0.685 microns. The dimension of the line width was about 5 microns.

5 Brief Description of 1.2-2.4 Micron Infrared Airborne Prototype System

We are developing a 1.2-2.4 μm , short-wave infrared P11 prototype system for USASSIC. After successful ground tests, the prototype system will be flown on the ASFTS C-130 plane based at the Eglin Air Force Base. The instrument will be mounted in the turret assembly and will observe selected targets on the ground.

The instrument will have one cooled focal plane array of 1 kgCdTe, manufactured by Rockwell. A specially designed optical configuration currently during manufacturing will be used in the system. The configuration allows the system to record simultaneously two polarization images side by side on the focal plane array. This approach is an economic approach, because of high cost of the focal plane array.

The system was designed to be a real-time instrument that will be able to collect an image cube data in seconds.

The system will use a TeO_2 AOTF designed and manufactured by Aurora Associates.

5.1 Important spectral features in this wavelength range

5.1.1 *Two major absorption bands due to H_2O and CO_2 in the Atmosphere*

There are two major absorption bands centered at 1.4 and 1.9 micron due to water and carbon dioxide molecules in the atmosphere. No useful solar radiation are available within the wavelength ranges of these two bands.

5.1.2 *Characteristic spectral signatures of man-made materials*

Nowadays, textures and paints are often made of synthetic materials, originally from petroleum products. These products often have characteristic spectral absorption features located at 1.7 and 2.3 microns. These two absorption bands occur in the atmosphere windows and are observable remotely. According to known spectra of organic materials, the spectral bands are likely vibration spectral Overtones of hydrocarbon polymers. Therefore, they could occur in many synthetic materials, such as paints, clothes, and plastic wares, as well as camouflaged clothes and painted surfaces. The similarity shows that observation of these spectral bands only implies detection of a man-made object, and not necessarily detection of a military target. However, this is a necessary classification process for distinguishing man-made objects from natural substances. Target shape and polarization properties could provide further evidence for detection and identification.

substances. Target shape and polarization properties could provide further evidence for detection and identification.

6 Acknowledgments

The work described in this paper was performed by the Center for Sparse Microelectronics Technology, Jet Propulsion Laboratory, California Institute of Technology, and was jointly sponsored by the Army Space Technology and Research Office, the Marine Corps System Command, Code AW, The Army Space and Strategic Defense Command and the National Aeronautics and Space Administration.

References

1. I.C.Chang, "Noncollinear Acousto-Optic Filter with Large Angle Aperture", *Appl.Phys.Lett.*, Vol. 25, p.370 (1974).
2. Li-Jen Cheng, Tien-Hsin Chao, Mack Dowdy, Clayton LaBar, Colin Mahoney, George Reyes, and Ken Bergman, "Multispectral Imaging Systems Using Acousto-Optic Tunable Filter", in "Infrared and Millimeter Wave Engineering", SPIE Proceedings Vol. 1874, p.224(1993).
3. Li-J. Cheng, M.K. Hamilton, J.C. Mahoney, G.F. Reyes "Analysis of AOTF Hyperspectral Imagery", in "Algorithms for Multispectral and Hyperspectral Imagery", SPIE Proceedings, Vol. 2231, p] 58-166 (1994).
4. Li. J. Cheng, J.C. Mahoney, G.F. Reyes, and H.R. Suiter, "Target Detection Using an AOTF Hyperspectral Imager", in "optical Pattern Recognition V", SPIE Proceedings, Vol. 2237, p.251-259 (1994).
5. Li-Jen Cheng and George Reyes, "Polarimetric Hyperspectral Imaging for Mine Detection", in "Detection Technologies for Mines and Minelike Targets", SPIE Proceedings, No. 2496, p.305 (1995)
6. Li-Jen Cheng, Guan-Pyng Li, and De Yu Zang "SoI Characterization Using AOTF Polarimetric Hyperspectral Imaging" Proceedings of 1994 IEEE International SOI Conference, October 3-6, 1994, Nantucket Island, MA.